

Zahorulko, A., Borsuk, S., Peczkis, G. (2022). Computational analysis of sealing and stability of a deformable floating and fixed rings of an annular seal. *Journal of Engineering Sciences*, Vol. 9(1), pp. D20-D29, doi: 10.21272/jes.2022.9(1).d4

## Computational Analysis of Sealing and Stability of a Deformable Floating and Fixed Rings of an Annular Seal

Zahorulko A.<sup>1</sup>[0000-0002-6198-4643], Borsuk S.<sup>1</sup>[0000-0002-1808-0008], Peczkis G.<sup>2</sup>[0000-0002-4856-3123]

<sup>1</sup> Sumy State University, 2, Rymaskogo-Korsakova St., 40007 Sumy, Ukraine;  
<sup>2</sup> Silesian University of Technology, 2A, Akademicka St., 44-100 Gliwice, Poland

### Article info:

Submitted: March 21, 2022  
 Accepted for publication: June 12, 2022  
 Available online: June 16, 2022

### \*Corresponding email:

[a.zagorulko@cm.sumdu.edu.ua](mailto:a.zagorulko@cm.sumdu.edu.ua)

**Abstract.** Solving the hydroelastic problem by using Ansys System Coupling (Mechanical and CFX) for floating and fixed rings of a deformable annular seal made it possible to analyze the influence of the cylindrical shell thickness, the inlet and outlet edge dimensions, inlet pressure, and shaft radial displacement on the hydrostatic pressure distribution and the clearance value on length, leakages, stress-strain state, and radial force. The analysis of static stability at an inlet pressure of 10 MPa for the basic seal design showed that the static radial force in the range of radial movements of the shaft from 0 to 50% of the clearance is centering, even though the inlet part of the seal clearance has a confusor, and the outlet part has diffuser form. However, the dynamic coefficients of the fixed sealing ring have a negative value of direct stiffness but positive values of direct and cross-coupled damping and cross-coupled stiffness. Verifying computational 2D and 3D models with experimental results from the literature showed that the maximum relative error does not exceed 10.7% for the hydrostatic pressure, 18% for the clearance, and 8.6% for the leakage value. Simultaneously, according to the trend, all calculated dependencies are identical to the experimental results.

**Keywords:** deformable annular seal, clearance, hydroelastic problem, sealing, stability.

## 1 Introduction

With industry development, the need for pumping and processing large masses of liquid and gaseous products is constantly growing [1]. One of the most critical problems in this area is the problem of creating reliable and hermetic seals. This situation is caused, on the one hand, by high sealing pressures and circumferential speeds, which increase yearly. On the other hand, stringent requirements for sealing and reliability rise along with the growth of parameters.

In modern pumping equipment, non-contact seals of the annular type have become widespread. The peculiarity of these seals is their direct influence on the vibration state of the rotors. Depending on the design of the seals, the hydrodynamic forces arising in them can have both a centering and decentering effect on the rotor. The main disadvantage of such seals is relatively large leakages of the pumped liquid, which reduce the efficiency of the pumps. Therefore, developing and calculating new designs of annular seals that provide

small leakages with the guaranteed non-contact operation of the rotor is an urgent and, at the same time, a difficult task, as it is necessary to find a compromise between these conflicting requirements. This provision determines the importance of research aimed at increasing the sealing capacity and vibration reliability of non-contact seals of rotors of high-speed pumps and reducing the complexity of calculations.

For the first time, the deformation problem of an annular seal was considered by Kamal [2]. He developed a simple method of analyzing the flow in an annular seal based on the solution of the Reynolds equation, considering the deformations of the shaft surfaces and the sealing ring as a part of the housing. Subsequently, Pick and Harris solved the hydroelastic problem for the so-called Morrison and Perry seals [3]. They used the finite element method to analyze the deformations of the ring shell and the shaft of the reciprocating joints. The pressure distribution in the seal, the movement of the sealing surfaces, and leakages were determined by the joint solution of the hydrodynamics equations and

elasticity using the successive approximations method. Khvorost, Melnyk, et al. [4] proposed a computational method for calculating the flow in a floating seal considering input losses. Yu.A. Kibets, in his dissertation [5], based on experimental studies, proposed a method for calculating deformable annular seals of turbopump units.

Recently, an increasing number of experimental [6, 7] and theoretical [8, 9] studies are related to analyzing the dynamics and leakages of floating seals of high-speed rotary machines such as aircraft engines, turbopump units, or gas turbines. Studies of static and dynamic lubrication parameters of bearings with floating rings for high-speed turbocompressors deserve special attention [10, 11, 12].

Therefore, this work aims to solve the hydroelastic problem and analyze the static and dynamic stability of the floating and fixed rings of the deformable annular seal of the high-speed turbopump. Verifying the computational model with experimental results from the literature [5].

## 2 Research Methodology

The hydroelastic problem for floating and fixed rings of a deformable annular seal was solved using Ansys System Coupling [13]. The analysis of ring deformations was performed in the Ansys Transient Structural module, and the calculation of fluid flow through the annular was conducted in the Ansys Fluid Flow (CFX) module.

The basic design of the deformable sealing ring (Fig.1) has the following dimensions and design parameters [5]:

- annular length  $l = 25$  mm;
- shaft diameter  $d = 120$  mm;
- radial clearance  $h_0 = 0.1$  mm;
- cylindrical shell thickness  $\delta = 2$  mm;
- inlet edge diameter  $D_1 = 155$  mm;
- inlet edge thickness  $b_1 = 5$  mm;
- outlet edge diameter  $D_2 = 155$  mm;
- outlet edge thickness  $b_2 = 5$  mm;
- $d_1 = 122$  mm;
- $d_2 = 126$  mm;
- $a = 1$  mm;
- undercutting diameter of outlet edge  $D = 130$  mm.

The material of the ring is bronze BrAlFeMg 10-3-2.

Computational studies were carried out for 2D and 3D models of sealing rings. For the 2D model, the static problem of analyzing the stress-strain state in an axisymmetric setting was considered. For the calculation 2D model hexa mesh of the ring and the clearance domain of the deformable floating seal, a sector with an angle of 5 degrees was chosen.

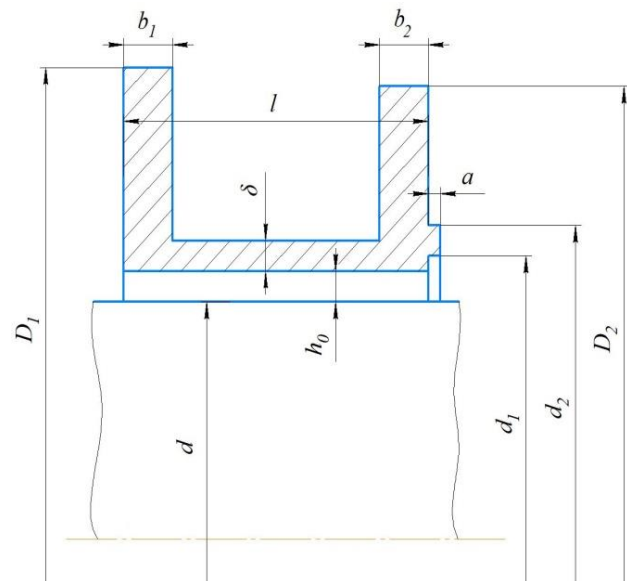


Figure 1 – Diagram of a deformable U-shaped sealing ring

The calculation mesh with boundary conditions is shown in Fig. 2 a,b. The size of the ring mesh is 17170 elements. The dimensionality of the liquid clearance mesh is 10,000 elements. As a boundary condition, the inlet pressure was set on the outer surface of the solid ring. The condition of rotational periodicity symmetry was applied to the side faces of the ring sector. The face surface frictional contact of the ring with the body was modeled with a friction coefficient of  $f=0.07$ . An interface for obtaining data on the hydrostatic pressure distribution and transmitting data on the distribution of the deformation was set on the inner surface. For the liquid clearance: on the side faces, the boundary conditions of rotational periodicity, static pressure at the inlet and outlet, on the surface of the shaft and the surface of the inner ring - conditions of the absence of sliding on the walls were set. In addition, on the surface connected to the inner surface of the ring, an interface for transmitting hydrostatic pressure distribution data and obtaining a strain distribution was determined.

A turbulent isothermal flow of water was considered using the  $k-\epsilon$  turbulence model. To model the boundary layer, the clearance mesh, which consisted of 10 elements in thickness, thickened near the walls. As a result of the calculations, hydrostatic pressure and clearance distributions along the seal length, the leakages, and the stress-strain state of the annular seal floating ring without considering the shaft rotation were obtained.

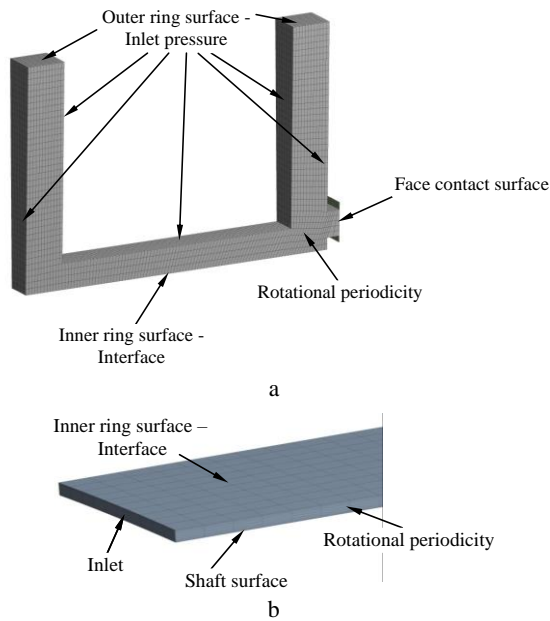


Figure 2 – Calculation mesh of the 2D model of the ring (a) and the clearance (b) of the deformable annular seal

For the 3D model, the complete rotational geometry of the sealing ring and liquid clearance with bonded contact of the face surface was considered. The calculated hexa mesh of the 3D model of the ring and the clearance is shown in Fig. 3a, b. The structured hexa mesh of the ring had 27607 elements, the clearance mesh - 30000. Similar to the 2D model, the inlet pressure was applied to the outer surface of the sealing ring as a boundary condition. A static sealing pressure was set at the inlet of the liquid clearance. Static pressure of 0 Pa was set at the outlet, which is the condition for the outflow of the liquid medium into the atmosphere. The inner cylindrical surfaces from the side of the ring and the clearance were used as interface surfaces. The condition of no sliding was set on the walls of the clearance.

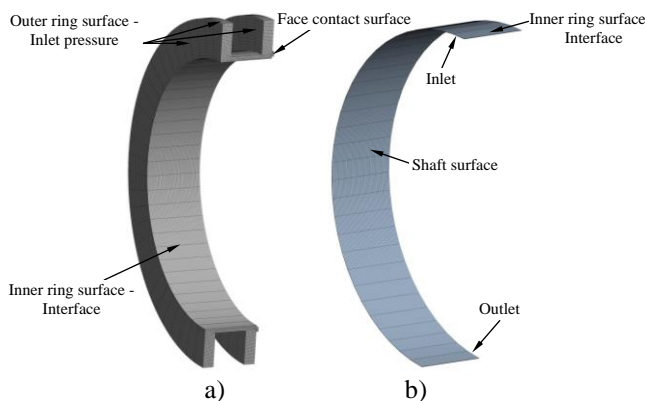


Figure 3 – Calculation mesh of the 3D model of the ring (a) and the clearance (b) of the deformable annular seal

The analysis of the static and dynamic stability of the shaft in the deformable annular seal was performed using the Ansys CFX numerical method of the deformed mesh.

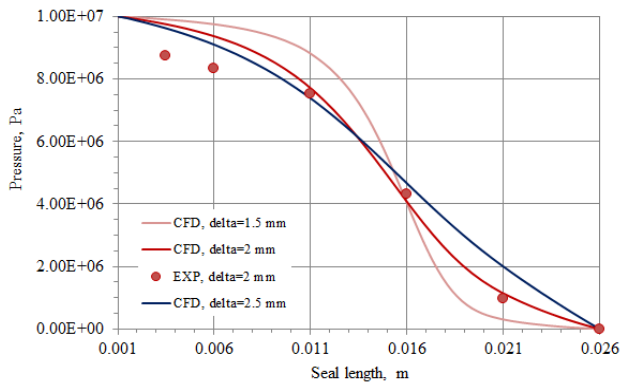
When analyzing the static stability of the floating and fixed rings of the deformable annular seal, a relative radial displacement  $e=0.2, 0.3, 0.4, 0.5$  was applied to the shaft surface depending on which the radial force and the leakages were obtained. The stress-strain state of the fixed ring of the deformable annular seal was analyzed.

When analyzing the dynamic state, with the fixed ring of the deformable annular seal, displacements  $z = e_z \cdot \cos(\omega t)$  and  $y = e_y \cdot \sin(\omega t)$  were applied to the shaft surface, which specified a direct synchronous whirl along a circular trajectory. At the same time, the rotational speed of the shaft surface was equal to 22,000 rpm. One shaft rotation with 20 timesteps was simulated. The eccentricity  $e_z = e_y = 0.01$  mm is equivalent to 10% of the clearance. As a result, the joint hydroelastic problem and shaft whirl along a circular trajectory was solved. Dynamic stiffness and damping coefficients were estimated using the hydrodynamic forces obtained during the calculation [14].

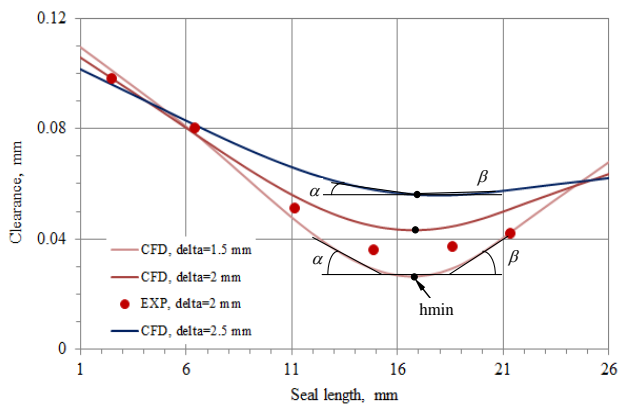
### 3 Results and Discussion

As a result of the static calculation for the floating and fixed rings of the deformable annular seal, the influence of the cylindrical shell thickness, the inlet and outlet edge dimensions, the inlet pressure, and the radial displacement of the shaft on the hydrostatic pressure and the clearance distributions along the length, leakages, the stress-strain state, and the radial force were analyzed.

The hydrostatic pressure and clearance distributions along the seal length at different cylindrical shell thicknesses (Fig. 4 a,b) show that for the 2D model of the basic design of the seal at  $\delta=2$  mm and the inlet-outlet edge thicknesses  $b_1=b_2=5$  mm, the calculation results agree well with the results of the experiment. Thus, the maximum relative error does not exceed 10.7% for hydrostatic pressure and does not exceed 18% for clearance. When the thickness of the cylindrical shell is reduced, the minimum clearance decreases by more than two times from  $h_{\min} = 0.0559$  mm to  $h_{\min} = 0.0265$  mm. Leakages reduce from  $Q = 1.33$  l/s to  $Q = 0.651$  l/s at  $\delta = 2.5$  mm and  $\delta = 1.5$  mm, respectively (Fig. 5). The profile of the hydrostatic pressure distribution is transformed from uniform close to parabolic to non-uniform with a convex shape of the curve on the confuser part of the clearance and a concave curve on the diffuser part of the clearance. The position of the minimum clearance slightly shifts towards the outlet to the seal.



a



b

Figure 4 – Hydrostatic pressure (a) and clearance (b) distributions along the length of the 2D model of the floating ring at the different cylindrical shell thicknesses

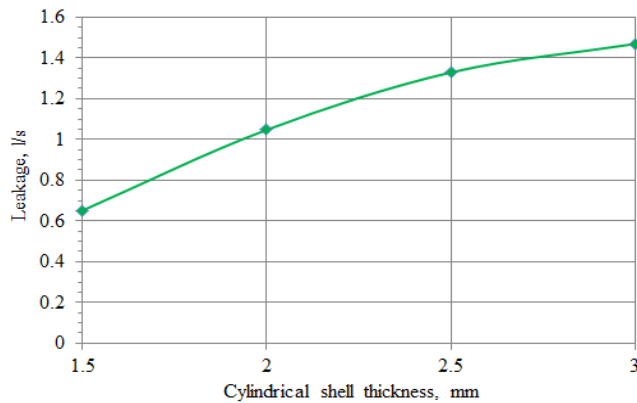
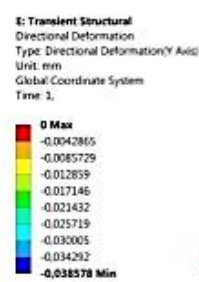


Figure 5 – Dependence of leakage on the cylindrical shell thickness for the 2D model of the floating ring

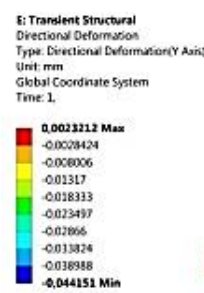
The radial deformations of the floating sealing ring (Fig. 6 a-d) show that when the thickness of the U-shaped cylindrical shell decreases, the angle of rotation  $\varphi$  increases, first of all, of the outlet edge. The opening angles of the confusor  $\alpha$  and diffuser  $\beta$  increase (Fig. 4b).

The hydrostatic pressure and clearance distributions along the length of the floating sealing ring (Fig. 7 a,b) show that as the inlet and outlet edge thicknesses

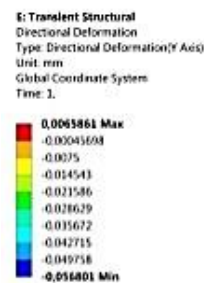
decrease, the pressure distribution profile fills up, and the minimum clearance decreases from  $h_{\min}=0.0416$  mm to  $h_{\min}=0.0319$  mm. Also, the position of the minimum clearance towards the outlet from the seal changes. With the inlet edge thickness  $b_1=3$  mm and  $b_1=1$  mm, and the outlet edge thickness  $b_2=1$  mm, a confusor shape of the clearance is provided along the entire seal length. Moreover, leakages have a minimum value of  $Q=0.77$  l/s (Fig. 8). Undercutting the outlet edge of the floating seal ring at  $b_1=b_2=5$  mm to a diameter of  $D=130$  mm also leads to the formation of a confusor clearance along the entire length of the seal. Leakages decrease from  $Q=1.048$  l/s to  $Q=0.875$  l/s. The hydrostatic pressure distribution profile has the most filled curve shape.



a



b



c

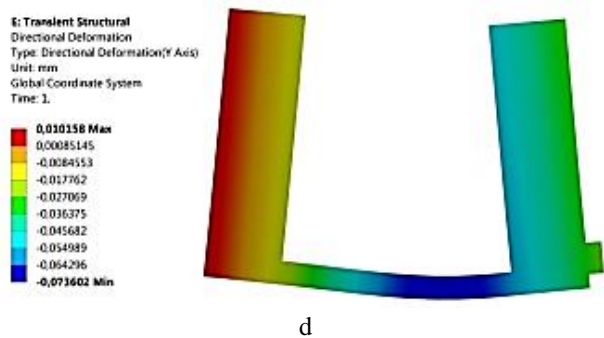
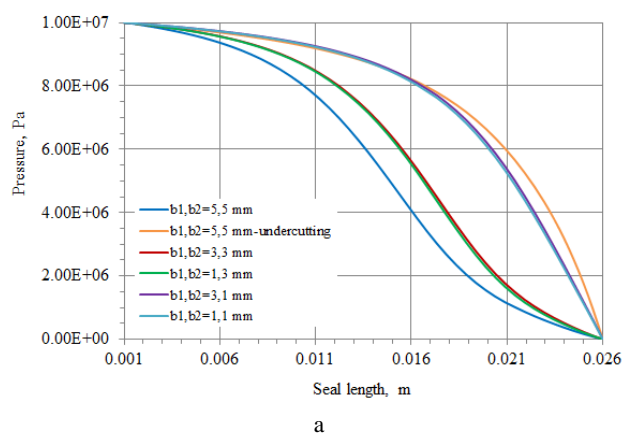
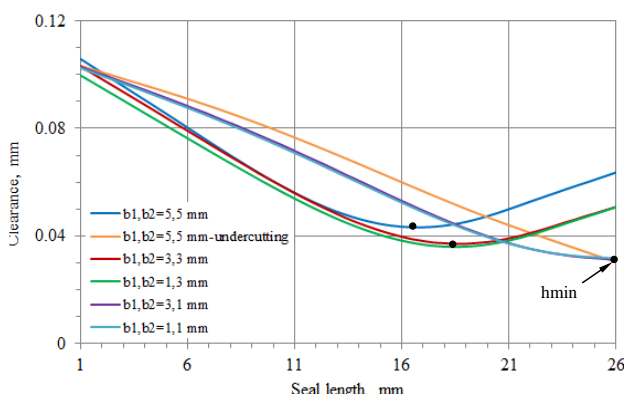


Figure 6 – Radial deformations of the 2D model of the deformable floating ring:  $\delta=3$  mm (a),  $\delta=2.5$  mm (b),  $\delta=2$  mm (c),  $\delta=1.5$  mm (d)

The radial deformations of the floating sealing ring (Fig. 9 a-f) increase with a decrease in the thickness of the inlet and outlet edges. Moreover, with a reduction in the output edge thickness and its undercutting, the value of the rotation angle of the input edge increases, and the value of the rotation angle of the output edge decreases. Thus, the primary influence on the cone-shaped deflection of the floating sealing ring is the thickness and diametrical size of the output edge.



a



b

Figure 7 – Hydrostatic pressure (a) and clearance (b) distributions along the length of the 2D model of the floating ring with different sizes of the inlet and outlet edges

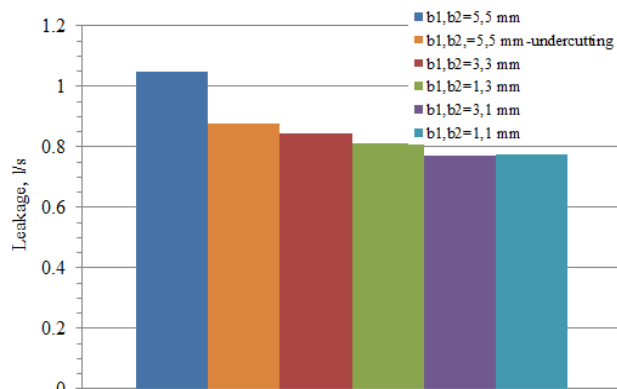
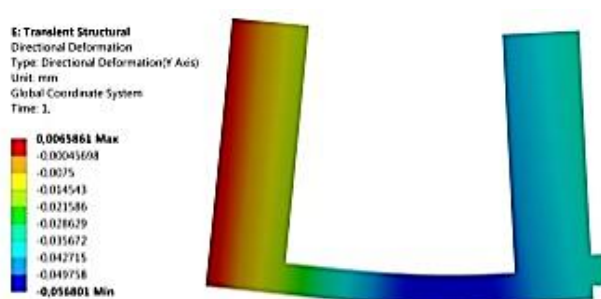
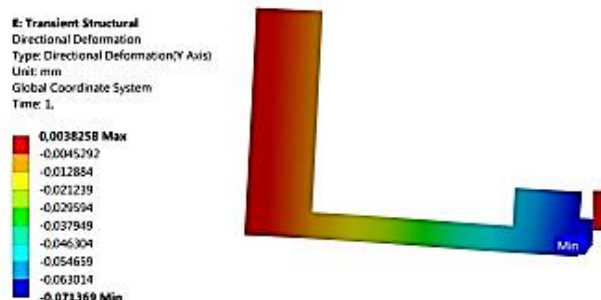


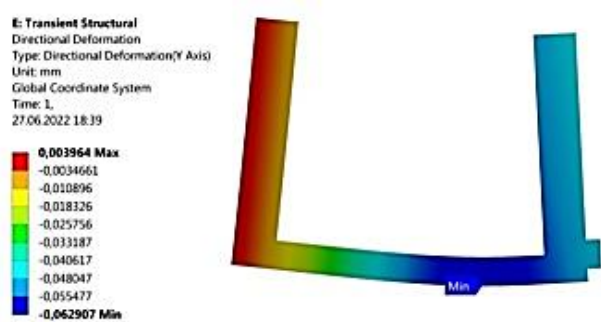
Figure 8 – Leakages in the 2D model of the floating ring with different sizes of the inlet and outlet edges



a



b



c

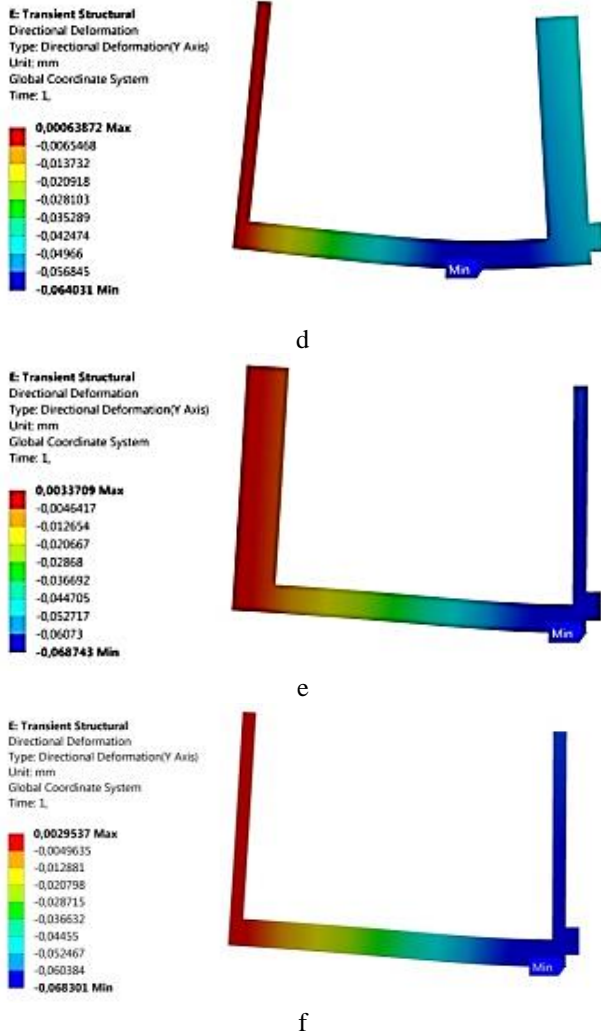


Figure 9 – Radial deformations of the 2D model of the deformable floating ring:  $b_1 = b_2 = 5$  mm (a),  $b_1 = b_2 = 5$  mm – undercutting (b),  $b_1 = b_2 = 3$  mm (c),  $b_1 = 1$  mm,  $b_2 = 3$  mm (d),  $b_1 = 3$  mm,  $b_2 = 1$  mm (e),  $b_1 = b_2 = 1$  mm (f)

Hydrostatic pressure and clearance distributions along the seal length depending on the sealing pressure for the basic design of the seal with a floating ring (Fig. 10 a, b) show an increase in the pressure profile and a decrease in the value of the minimum clearance with an increase in the inlet pressure. The gap size decreases almost twice from  $h_{\min} = 0.0872$  mm to  $h_{\min} = 0.0432$  mm at  $P_{\text{in}} = 2$  and 10 MPa, respectively.

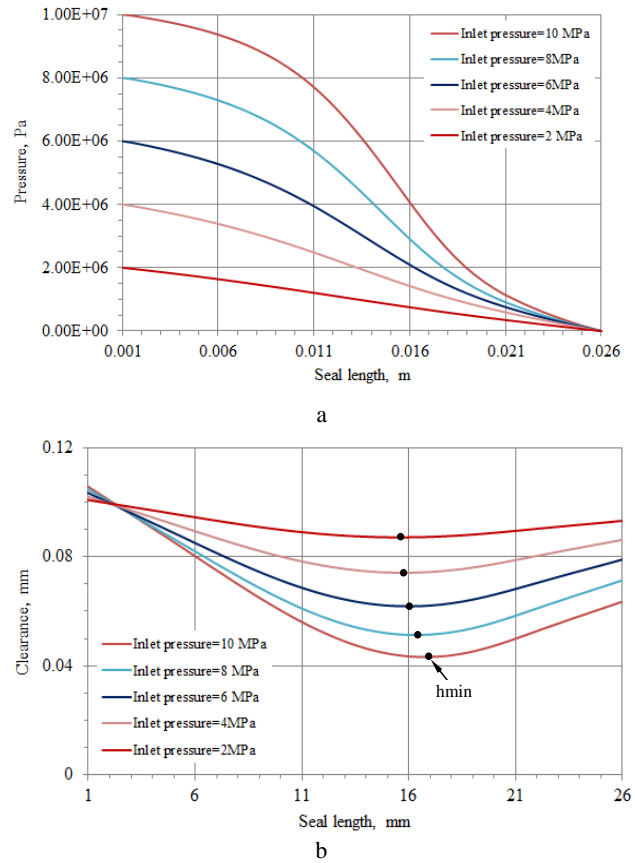


Figure 10 – Hydrostatic pressure (a) and clearance (b) distributions along the length of the 2D model of the deformable floating ring at different sealing pressures for the basic seal design ( $\delta = 2$  mm,  $b_1 = b_2 = 5$  mm)

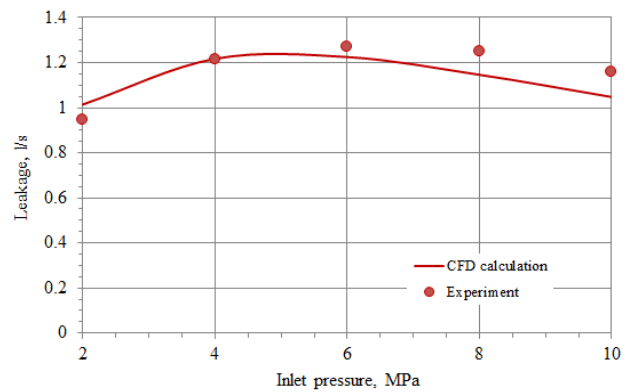


Figure 11 – Leakages depending on the inlet pressure in the 2D model of the deformable floating ring of the basic seal design ( $\delta = 2$  mm,  $b_1 = b_2 = 5$  mm)

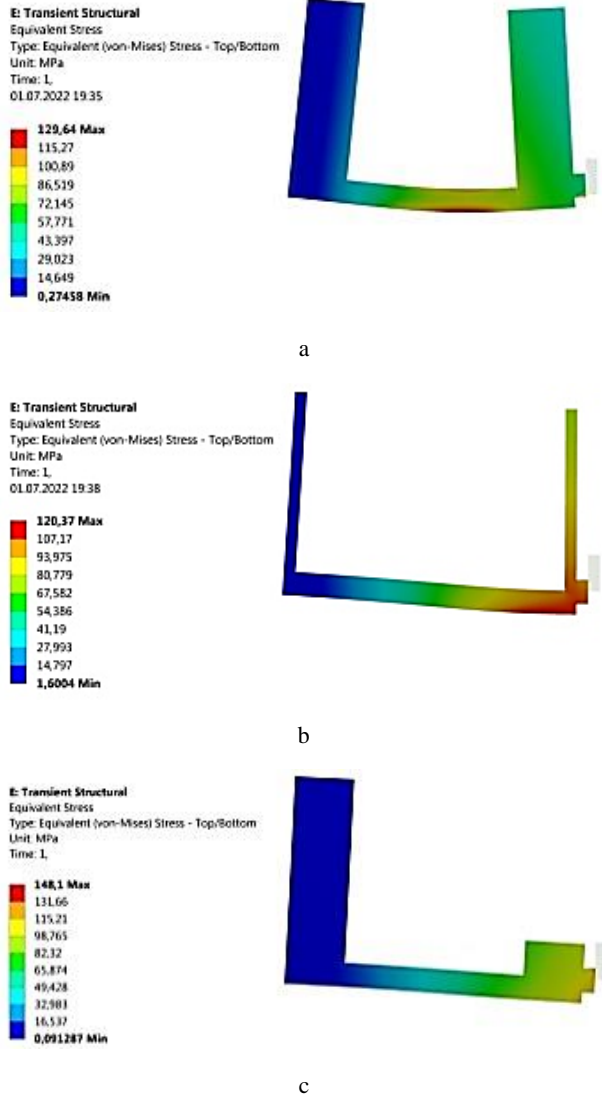


Figure 12 – Equivalent stresses in the basic design  $b_1=b_2=5$  mm (a), design with  $b_1=b_2=1$  mm (b), and design with undercutting  $b_1=b_2=5$  mm (c) 2D model of seal

Also, the minimum clearance position slightly shifts towards the outlet from the seal. This fact explains the quadratic change in the leakages from the sealing pressure (Fig. 11). First, there is an increase in leakage up to a pressure value of approximately 6 MPa, and then the leakage value begins to decrease at pressures of 8 and 10 MPa. The relative error between calculated and experimental data on the leakages does not exceed 8.6%. At the same time, according to the trend, all calculated dependences are identical to the experimental results.

It is clear that the radial deformations of the floating ring of the basic design increase with increasing inlet pressure. A comparison of the equivalent stresses at an inlet pressure of  $P_{in}=10$  MPa (Fig. 12) for the basic design, a design with minimal thickness of the inlet and outlet edges, and a design with undercutting of the outlet edge showed that the most significant value of stress is in the design with undercutting of the outlet edge.

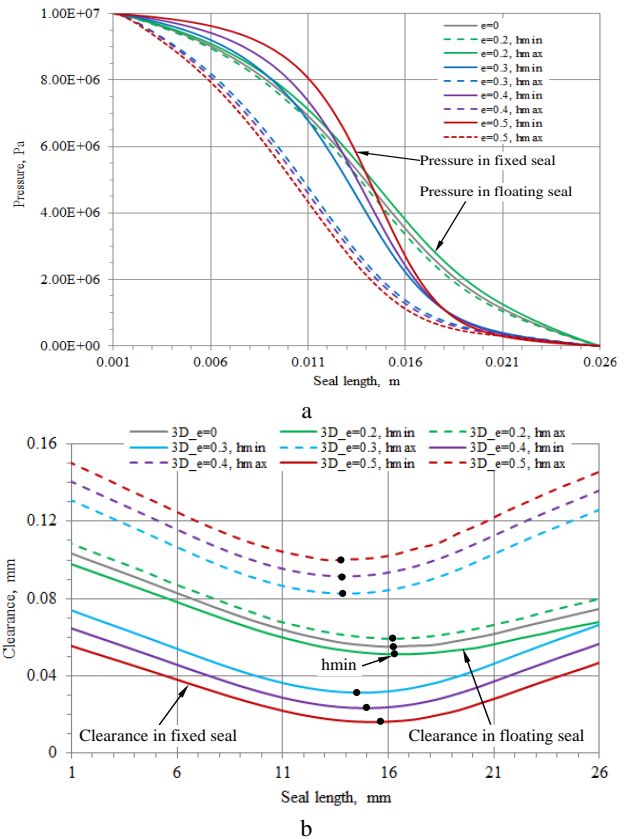


Figure 13 – Hydrostatic pressure (a) and clearance (b) distributions along the length of the 3D model of the deformable floating and fixed rings at different shaft radial displacements

Moreover, the equivalent stresses are significantly lower than the allowable stress for the material of 340 MPa.

Hydrostatic pressure and clearance distributions along the length of floating and fixed deformable seal rings at different shaft radial displacements (Fig. 13 a, b) show that for the 3D model of the floating ring, the difference between pressure and clearance distributions in the places of minimum and maximum clearances is insignificant. This is because, with a relative radial displacement of the shaft  $e=0.2$ , the radial hydrostatic force in the seal displaces the ring in the reverse direction by  $e=0.16$ . That is, by approximately 80% of the previous radial displacement of the shaft. At the same time, the radial force is equal to 521.2 N, and the frictional force in the contact of the floating ring is equal to 453.3 N (Fig. 14 b). And this means that the radial force is only 13% more than the friction force. At the same time, the amount of leakages  $Q=1.36$  l/s almost does not change, and the amount of radial force increases significantly less than for a fixed ring if compared with the concentric position of the shaft  $e=0$  (Fig. 14 a,b). But on the contrary, for a fixed ring, the difference between the hydrostatic pressure and clearance distributions in the places of minimum and maximum clearances is significant and is associated with a more substantial radial displacement of

the shaft  $e=0.3, 0.4, 0.5$  (Fig. 13 a,b). The minimum clearance varies in size and position along the seal length (Fig. 13 b), which is explained by the difference between the hydrostatic pressure profiles. The increase in leakage and radial force from the radial displacement of the shaft for the design of the seal with a fixed deformable ring occurs according to linear dependencies (Fig. 14 a,b).

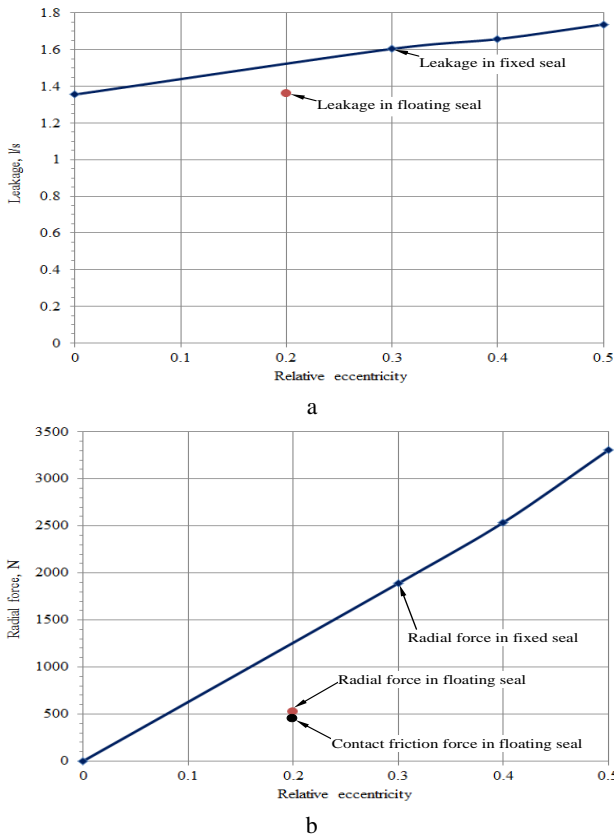
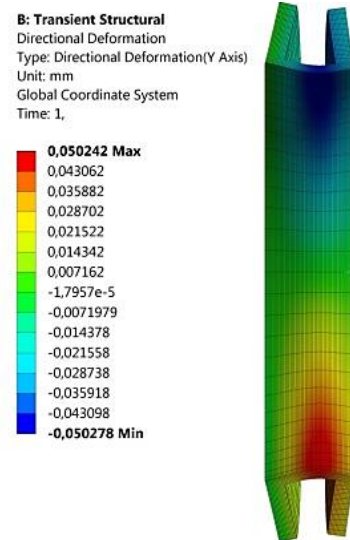


Figure 14 – Dependence of leakage (a) and radial force (b) on the shaft radial displacement for a 3D model of deformable floating and fixed annular seal rings

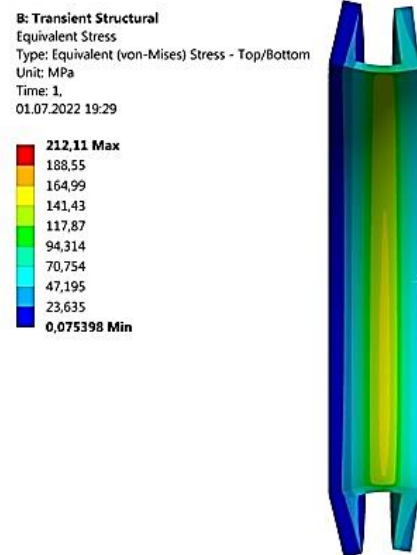
Fixation of the deformable sealing ring is because with an increase in the relative radial displacement of the shaft, there is an increase in the radial force that tries to move the ring in the opposite direction, which leads to significant deformations of the calculation mesh and this makes it impossible to perform further calculations.

Radial displacement and equivalent stresses of the 3D model of the sealing ring are presented in Figures 15 a, b.

A comparison of the radial deformations of the static and fixed dynamic 3D models (Fig. 16 a,b) shows that a more significant amount of deformation and movement of the minimum clearance position towards the seal outlet occurs in the static model. This is because the floating ring in the static model can move the face contact surface, unlike the fixed ring in the dynamic model. However, the dynamic model of the undercutting ring design (Fig. 16 c) has the most considerable deformation, even though the ring is fixed.

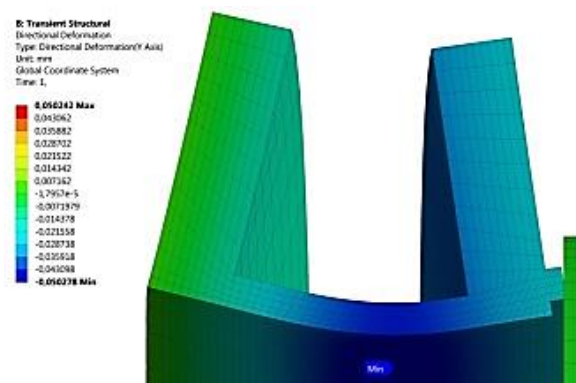


a

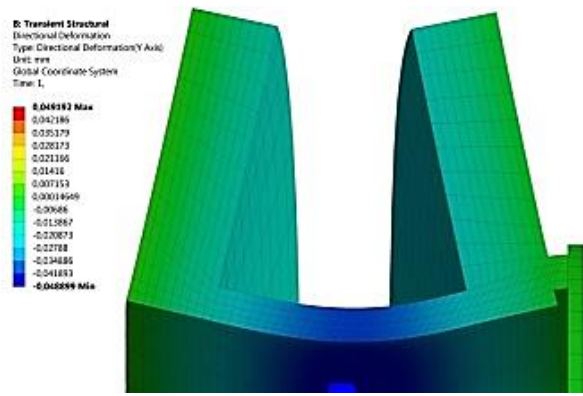


b

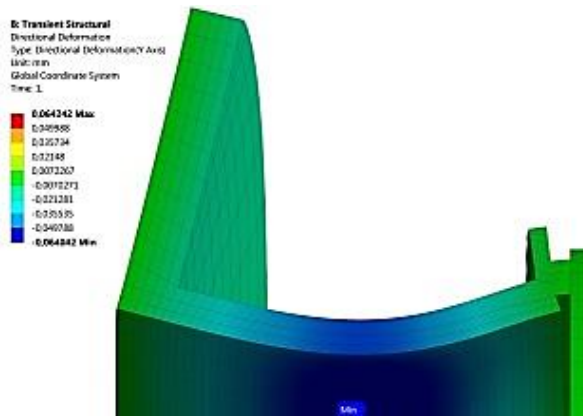
Figure 15 – Radial deformations (a) and equivalent stresses (b) of the 3D model of the deformable floating ring at  $e = 0.2$



a



b



c

Figure 16 – Radial deformations of static (a) and fixed dynamic 3D models of the basic design  $b_1 = b_2 = 5$  mm (b) and design with undercutting  $b_1 = 3$  mm,  $b_2 = 1$  mm (c)

As a result of a dynamic calculation, based on hydrodynamic forces in the clearance of the deformable fixed ring of the annular seal, the coefficients of direct and cross-coupled stiffness and damping were estimated. The minimum clearances and leakages in the basic design and the design with undercutting  $b_1=3$  mm,  $b_2=1$  mm were obtained (Table 1, Fig. 16 b,c).

Table 1 – Dynamic coefficients, leakages, and minimum clearances for two designs of deformable annular seals

Design, mm	k, N/m	C, N·s/m	-K, N/m	c, N·s/m	Q, l/s	$h_{min}$ , mm
$b_1=b_2=5$ , $\delta=2$	7.94e7	4.75e8	2.36e8	7.22e8	1.3	0.05
$b_1=3$ , $b_2=1$ (under-cutting) $\delta=2$	1.00e8	6.00e8	3.00e08	8.00e8	1.0	0.04

Both designs have a negative coefficient of direct stiffness and positive coefficients of direct and cross-coupled damping and cross-coupled stiffness. This indicates the dynamic stability of the shaft in these seals. However, the negative direct stiffness must be considered when calculating the critical shaft speed. In the

undercutting design, the absolute values of all dynamic coefficients increase, which is associated with a decrease in the clearance and, accordingly, the amount of leakages. The negative stiffness coefficient is due to an increase in the total velocity of the fluid flow in the place with the minimum clearance (Fig. 17).

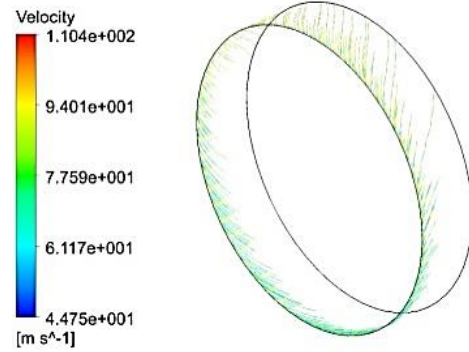


Figure 17 – Streamlines velocity in a 3D dynamic model of a fixed ring of a deformable annular seal

#### 4 Conclusions

Solving the hydroelastic problem by using Ansys System Coupling (Mechanical and CFX) for floating and fixed rings of a deformable annular seal made it possible to analyze the influence of the cylindrical shell thickness, the inlet and outlet edge dimensions, inlet pressure, and shaft radial displacement on the hydrostatic pressure and the clearance distributions along the length, leakages, stress-strain state, and radial force.

Verification of computational 2D and 3D models with experimental results known from the literature showed that the maximum relative error does not exceed 10.7% for the hydrostatic pressure, 18% for the clearance, and 8.6% for the leakages. At the same time, according to the trend, all calculated dependencies are identical to the experimental results. Some slight discrepancy between the calculation and the experiment results is explained by the simulation being performed without considering the pressure losses at the seal inlet.

The calculation studies showed that due to the deformations of the U-shaped ring under the sealing pressure, the clearance and leakages in the deformable seal are significantly reduced. By selecting the cylindrical shell thickness and the inlet and outlet edge thicknesses, it is possible to influence the size and the clearance shape between the shaft and the ring. Reducing the cylindrical shell thickness reduces the minimum clearance size and increases the opening angle of the confuser and diffuser channels, which are formed at the inlet and outlet parts of the seal. Reducing the inlet and outlet edge thickness reduces the minimum clearance value and increases the confuser clearance length. This occurs due to deformations and movement of the face contact surface in the radial direction to the shaft surface. The formation of a confuser clearance along the entire seal length also

ensures a separate reduction in thickness and undercutting of the outlet edge of the deformable seal. In this case, leakages are visibly reduced.

An increase in the sealing pressure for the basic design of the seal naturally leads to a decrease in the minimum clearance value due to the deflection of the cylindrical shell and the radial movement of the face contact surface. The opening angles of the confuser and diffuser increase. Leakages initially increase to a pressure value of 6 MPa and then decrease. The curve has a parabolic shape.

The maximum stresses for all considered designs of the deformable annular seal do not exceed the maximum allowable material stress of 340 MPa.

In the static analysis, at an input pressure of 10 MPa and a radial displacement of the shaft  $e=0.2$ , self-centering of the floating sealing ring occurs under the action of a centering radial force. An increase in the shaft radial displacement from  $e=0.3$  to  $e=0.5$  in a seal with a fixed ring leads to a linear increase in the centering radial force and leakages. Static stability is ensured even in the presence of confuser and diffuser clearances regions along the length of the seal.

The analysis of the dynamic stiffness and damping coefficients for the fixed ring of the deformable seal of

the basic design with the input and output edges thickness of 5 mm and the design with the input edge thickness of 3 mm and output edge thickness of 1 mm with undercutting shows the presence of a negative value of direct stiffness, which is caused by an increase in the total velocity of the fluid flow in the place of the minimum clearance. At the same time, reducing the thickness of the edges reduces the value of the minimum clearance and leads to an increase in the absolute value of the dynamic coefficients of direct and cross-coupled stiffness and damping. Regardless of the negative direct stiffness, the dynamic stability of the seal is ensured. However, the negative value of direct stiffness must be considered when calculating the critical shaft rotation speed.

## 5 Acknowledgments

The Sumy State University supported this article. Project: Research on the “Analysis of the Influence of Hydrodynamic Forces Acting in Narrow Clearances of Seals and Bearings on Increasing Energy Efficiency and Reducing the Harmful Emissions and Vibrations of Centrifugal Machines” (0120U102004) of Sumy State University funded by the Ministry of Education and Science of Ukraine.

## References

1. Martsynkovskyy V.A. (2005). Hermomechanics, its role in ensuring the efficiency and environmental friendliness of pumping and compressor equipment. *Bulletin of Sumy State University, Series “Technical Sciences”*, Vol. 1(73), pp. 5–10.
2. Kamal, M. M. (1968). A high pressure clearance seal. *ASME. J. of Lubrication Tech.*, Vol. 90(2), pp. 412–416, doi: 10.1115/1.3601575.
3. Pick, R. J., Harris, H. D. (1980). Morrison and parry seals for water pressures up to 345 MPa. *J. Pressure Vessel Technol.*, Vol. 102(1), pp. 84–89, doi: 10.1115/1.3263306.
4. Khvorost, V. A., Pryadko, S. V., Mel'nik, V. A. et al. (1987). Method of calculating floating seals. *Vestn. Mashinotr.*, Vol. 6, pp. 23–25.
5. Kibets, Yu.A. (1988). Development of methods for calculating deformable annular seals of turbopump units. CSc. thesis. Kharkiv, Ukraine.
6. Arghir M. (2015). Experimental study of floating ring annular seals using high-speed optical techniques and mark tracking methods. *CFM 2015 - 22ème Congrès Français de Mécanique*. Lyon, France.
7. Li, G., Zhang, Q., Huang, E., Lei, Z., Wu, H., Xu, G. (2019). Leakage performance of floating ring seal in cold/hot state for aero-engine. *Chinese J Aeronaut*, Vol. 32, pp. 2085–2094, doi: 10.1016/j.cja.2019.03.004.
8. Ha, T.-W., Lee, Y.-B., Kim, C.-H. (2002). Leakage and rotordynamic analysis of a high pressure floating ring seal in the turbo pump unit of a liquid rocket engine. *Tribol Int*, Vol. 35, pp. 153–61, doi: 10.1016/S0301-679X(01)00110-4.
9. Duan, W., Chu, F., Kim, C.-H., Lee, Y.-B. (2007). A bulk-flow analysis of static and dynamic characteristics of floating ring seals. *Tribol Int*, Vol. 40, pp. 470–480, doi: 10.1016/j.triboint.2006.04.010.
10. Xie, Z., Zhu, W. (2022). An investigation on the lubrication characteristics of floating ring bearing with consideration of multi-coupling factors. *Mech Syst Signal Process*, Vol. 162, 108086, doi: 10.1016/j.ymsp.2021.108086.
11. Zhang, Y., Wang, W., Wei, D., Wang, G., Xu, J., Liu, K. (2022). Coupling analysis of tribological and dynamical behavior for a thermal turbulent fluid lubricated floating ring bearing-rotor system at ultra-high speeds. *Tribol Int*, Vol. 165, 107325, doi: 10.1016/j.triboint.2021.107325.
12. Novotný, P., Škara, P., Hliník, J. (2018). The effective computational model of the hydrodynamics journal floating ring bearing for simulations of long transient regimes of turbocharger rotor dynamics. *Int J Mech Sci*, Vol. 148, pp. 611–619, doi: 10.1016/j.ijmecsci.2018.09.025.
13. Workbench User's Guide, Release 18.2, ANSYS Inc., 2017.
14. Zahorulko, A. V., Gerasimiva, K. P., Altyntsev, E. I., Hudkov, S. N. (2009). Computer modeling of the spatial flow in the annular channel of the annular seal-bearing. *Eastern European Journal of Advanced Technologies*, Vol. 6/7(42), pp. 22–26.